Accepted Manuscript

Structure and permanent magnet properties of $Zr_{1-x}R_xFe_{10}Si_2$ alloys with R = Y, La, Ce, Pr and Sm

A.M. Gabay, R. Cabassi, S. Fabbrici, F. Albertini, G.C. Hadjipanayis

PII: S0925-8388(16)31417-7

DOI: 10.1016/j.jallcom.2016.05.092

Reference: JALCOM 37611

To appear in: *Journal of Alloys and Compounds*

Received Date: 21 February 2016

Revised Date: 19 April 2016

Accepted Date: 9 May 2016

Please cite this article as: A.M. Gabay, R. Cabassi, S. Fabbrici, F. Albertini, G.C. Hadjipanayis, Structure and permanent magnet properties of $Zr_{1-x}R_xFe_{10}Si_2$ alloys with R = Y, La, Ce, Pr and Sm, *Journal of Alloys and Compounds* (2016), doi: 10.1016/j.jallcom.2016.05.092.

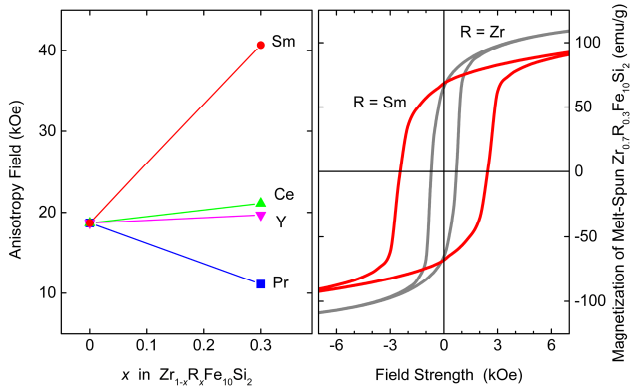

Structure and permanent magnet properties of $Zr_{1-x}R_xFe_{10}Si_2$ alloys with R = Y, La, Ce, Pr and Sm

A.M. Gabay,[1*] R. Cabassi,[2] S. Fabbrici,[2] F. Albertini,[2] G.C. Hadjipanayis[1]

[1]Department of Physics and Astronomy, University of Delaware, 217 Sharp Lab, Newark, Delaware, 19716, USA

[2]IMEM-CNR, Parco Area delle Scienze 37/A, Parma 43124, Italy

Arc-melted $(Zr_{0.7}R_{0.3})_{1.1}Fe_{10}Si_2$ alloys with R = Y, Ce, Pr and Sm crystallize into the $ThMn_{12}$-type structure; La substitution leads to the formation of a separate $NaZn_{13}$-type phase. Compared to the rare-earth-free parent compound, Y, Ce and Sm strengthen the magnetocrystalline anisotropy in this order; whereas Pr weakens it. The effect of Sm is by far the strongest; an anisotropy field of 40.7 kOe determined for the $Zr_{0.7}Sm_{0.3}Fe_{10}Si_2$ by the singular point detection technique is high enough to make this compound a good candidate for a very rare-earth-lean, cobalt-free permanent magnet material. The effect of Sm has been demonstrated in isotropic nanocrystalline alloys prepared via melt-spinning followed by vacuum annealing. The optimally processed alloys with R represented by Zr and Sm exhibited coercivity values of 0.7 and 2.4 kOe, respectively. The analysis suggests that the development of the coercivity is controlled by decomposition of the 1:12 structure in the former sample and by the crystallite growth in the latter. Calculated remanence and maximum energy product of the Sm-substituted nanocrystalline alloy were 6.3 kG and 4.6 MGOe. The cubic $Zr_6Fe_{16}Si_7$ compound, which is the frequent minority phase in the studied alloys, was also synthesized and found to be paramagnetic at the room temperature.

Keywords: intermetallics; rare earth alloys and compounds; crystal structure; anisotropy; rapid quenching; permanent magnets

---

*Corresponding author. Address: University of Delaware, 217 Sharp Lab, Newark, DE 19716, USA. Tel.: +1 (302) 831 6345

E-mail address: gabay@udel.edu (A.M. Gabay).

1. Introduction

$ThMn_{12}$ (hereafter, 1:12) is one of several structure types derived from the hexagonal $CaCu_5$ by replacing part of its large atoms with pairs of smaller ones. When the replacement is random, it occurs as in a solid solution (this solid solution is often associated with the $TbCu_7$ prototype); however, additional ordering of the substituting atom pairs produces stoichiometric structures such as the rhombohedral Th_2Zn_{17} and tetragonal 1:12. Many of the iron-rich 1:12 compounds represented by the formula $R(Fe,M)_{12}$, where R is the rare earth and M is one of the transition metals or *sp* elements stabilizing the structure, exhibit not only a room-temperature ferromagnetism but also a significant uniaxial magnetic anisotropy [1]. At least three subgroups of such compounds have been considered for permanent magnet applications: $Sm(Fe,M)_{12}$ [2-4], $Nd(Fe,M)_{12}N_x$ [5-7] and, more recently, $Ce(Fe,M)_{12}$ [8-10]. The supply risks currently associated with the rare earth elements [11] increase the appeal of these rare earth-lean compounds, especially those not containing the high-demand neodymium. According to the latest finding [12], the $R(Fe,Si)_{12}$ compound can even be rare-earth-free having the R element represented by zirconium. The metastable $ZrFe_{10}Si_2$ exhibits fairly high values of Curie temperature (325 °C) and saturation magnetization (at least 11 kG), but it lacks a strong magnetocristalline anisotropy. Its room-temperature anisotropy field H_a was found to be only 17 kOe [12], which is especially low compared to nearly 120 kOe reported for $SmFe_{10}Si_2$ [13]. Since a high H_a is generally necessary for the development of a functional permanent magnet, in this work we attempted to increase it by partially substituting Zr with Y, La, Ce, Pr and Sm. The effect of the Sm substitution was further evaluated by comparing the magnetic behavior of nanocrystalline $ZrFe_{10}Si_2$ and $Zr_{0.7}Sm_{0.3}Fe_{10}Si_2$ alloys prepared via melt-spinning.

2. Experiment

Alloys $Zr_{5.9}R_{2.5}Fe_{76.2}Si_{15.4} = (Zr_{0.7}R_{0.3})_{1.1}Fe_{10}Si_2$, were prepared for R = Zr, Y, La, Ce, Pr and Sm by arc-melting the pure components in a water-cooled copper hearth. A Sm charge of 112% the nominal mass was required to offset the evaporation loss of this volatile element. The ingots (2.5 g or 10 g for R = Zr, Sm) were not subjected to any additional heat treatment. The alloy densities measured via the water-immersion technique were 7.26 (R = Zr), 7.17 (Y), 7.31 (Ce), 7.31 (Pr) and 7.33 (Sm) g/cc. In addition, a $Zr_{20.7}Fe_{55.2}Si_{24.1}$ alloy was prepared by arc-melting and annealed at 1100 °C for up to 60 h to obtain the frequently observed impurity phase

$Zr_6Fe_{16}Si_7$. Melt-spinning was done in argon by ejecting the inductively melted alloys onto a rotating copper wheel at a surface velocity v_s ranging from 5 to 25 m/s. Some of the melt-spun "ribbons" were annealed in a 10^{-4} Torr vacuum at 600 – 900 °C for 5 – 100 min.

Powder X-ray diffraction (XRD) characterization was performed with a Rigaku Ultima IV diffractometer using the CuKα radiation; the results were analyzed with Powder Cell software [14]. Minority phases were additionally analyzed in polished unetched samples with scanning electron microscopy (SEM; a JEOL JSM-6335F instrument) and energy-dispersive spectrometry (EDS; an IXRF Systems instrument). The crystallites in the ribbons were observed on freshly fractured surfaces. Magnetic anisotropy fields were determined via the singular point detection technique (SPD) [15] which is particularly convenient and accurate for polycrystalline samples. In the SPD, a pulsed magnetic field is applied to the sample and the anisotropy field is detected as a singularity in the second derivative of magnetization. The rise time of the pulse was 0.5 ms, and the $d^2M/dH^2(H)$ was obtained through analog derivation. The magnetization measurements were done with a Quantum Design VersaLab vibrating sample magnetometer (maximum field 30 kOe). Magnetization as a function of temperature was recorded at a field of 5 kOe. Magnetic hysteresis of the melt-spun ribbons was recorded along the ribbon length, thus ensuring a negligible self-demagnetization.

3. Results and discussion

3.1. Synthesis of $Zr_{0.7}R_{0.3}Fe_{10}Si_2$ compounds and their properties

The XRD data collected for the mortar-ground $Zr_{5.9}R_{2.5}Fe_{76.2}Si_{15.4}$ alloys are presented in Fig. 1. The spectrum for the parent $Zr_{8.4}Fe_{76.2}Si_{15.4}$ alloy reported in Ref. 12 was consistent with coexistence of the principal 1:12 structure and 3.7 vol. % of a $Zr_6Fe_{16}Si_7$ minority phase (the $Mg_6Cu_{16}Si_7$ type, a derivative of the Th_6Mn_{23} type; space group $Fm\bar{3}m$). A significant deviation from this phase composition can only be seen for R = La. A large amount of the cubic $NaZn_{13}$-type structure (space group $Fm\bar{3}c$) present in this alloy almost certainly manifests formation of the well-known $La(Fe,Si)_{13}$ phase [16]. There are no indications that the La atoms substitute for Zr in the $ZrFe_{10}Si_2$ structure. For the other examined rare earth elements, the 1:12 structure remains the predominant phase (96.3 – 98.5 vol. %), and both its lattice parameters – they are listed in Table I – increase compared to the unsubstituted material. This behavior implies that the Y, Ce, Pr and Sm atoms replace part of the smaller Zr atoms. The second detected phase is either

the cubic $Zr_6Fe_{16}Si_7$ or, in the case of R = Pr, the tetragonal $PrFe_2Si_2$ phase (the $BaAl_4$ type, I4/mmm, a = 0.399 nm, c = 1.005 nm).

To accurately determine the saturation magnetization of the 1:12 compounds, the impurity phases had to be accounted for. The $PrFe_2Si_2$ compound is known to be paramagnetic at room temperature (it orders antiferromagnetically at 7.7 K [17]). No past reports could be found, however, on the magnetism of the $Zr_6Fe_{16}Si_7$ compound. Therefore, after verifying with the EDS that this minority phase does not accommodate the rare earth atoms, we proceeded to synthesize it for magnetic characterization. The cubic $Zr_6Fe_{16}Si_7$ phase was not the main phase in the *as-prepared* alloy of this composition, and as many as four other phases (the 1:12, bcc Fe-Si, ZrFeSi and $ZrFe_4Si_2$) were detected at the different stages of the alloy equilibration at 1100 °C. Figure 2a presents an XRD spectrum recorded after annealing for 60 h, when the $Zr_6Fe_{16}Si_7$ had become the principal phase. The $M(H)$ curve shown in Fig. 2b suggests that at room temperature this main phase is paramagnetic. The small, 0.07 emu/g, ferromagnetic component of the alloy magnetization is likely to be caused by a trace amount of the bcc Fe-Si phase.

Table I presents the room-temperature magnetic properties and Curie temperatures of the five studied $Zr_{0.7}R_{0.3}Fe_{10}Si_2$ compounds. The saturation magnetization $4\pi M_s$ of the corresponding $Zr_{5.6}R_{2.5}Fe_{76.2}Si_{15.4}$ alloys was determined by extrapolating the $M(1/H^2)$ data for the field-oriented alloy powders. These findings were then corrected for the volume occupied by the impurity phases. Anisotropy field values were obtained from the positions of the d^2M/dH^2(H) peaks (see Fig. 3) after correction for the self-demagnetization.

The $4\pi M_s$ and H_a values presented here for the parent $ZrFe_{10}Si_2$ compound are slightly higher than in Ref. 12; the difference reflects, respectively, the correction for the imperfect purity and the use of the SPD. The effect of the 30% rare earth substitution for Zr on the $4\pi M_s$ is limited to only a few percent. In contrast, the H_a undergoes dramatic changes such as a nearly 40% decline for R = Pr and a 120% increase for R = Sm. The strong positive effect of the Sm substitution on the uniaxial anisotropy and the negative effect of the Pr substitution are consistent with the negative crystal field parameter A_{20} of the R sublattice in the $R(Fe,M)_{12}$ compounds and the positive (negative) second-order Stevens coefficient of Sm (Pr) [1]. The last column in Table I presents calculated values of the magnetic hardness parameter $(H_a/8\pi M_s)^{1/2}$ proposed [18] as a measure of whether the material can be developed into an efficient permanent magnet. The "passing" value of this parameter is 1, and small modifications of the rare earth-free $ZrFe_{10}Si_2$

with Y and Ce do not improve the application prospects of this compound, even though they do increase the H_a. On the other hand, a very moderate Sm substitution amounting to the total of only 2.3 at.% Sm allows for a permanent-magnet-grade "hardness" in the $Zr_{0.7}Sm_{0.3}Fe_{10}Si_2$. With so little rare earth, no cobalt and the upper limit of the magnetic energy product $4\pi^2 M_s^2$ of 34.8 MGOe, the $Zr_{1-x}Sm_xFe_{10}Si_2$ appears to be worth considering for filling the "gap" existing between the very inexpensive ferrite magnets and the much costlier magnets based on Nd-Fe-B and Sm-Co. The past experience does not suggest that it will be easy to develop functional permanent magnet properties in this case: only a 4 kOe coercivity was reported for the nanocrystalline $SmFe_{10}Si_2$ alloy [19]; this is 3.3% of the corresponding anisotropy field of 120 kOe [13].

3.2. Hard magnetic properties of melt-spun alloys for R = Zr, Sm

Figure 4 presents some of XRD spectra recorded for the two melt-spun alloys; prior to this characterization the alloys had been ground with a hand mortar. Compared to arc-melting, melt-spinning at relatively low solidification rates (corresponding to the v_s of 5 – 10 m/s) produces a somewhat *less* pure $ZrFe_{10}Si_2$ compound (with the additional impurity phase of the bcc Fe-Si) and a *more* pure $Zr_{0.7}Sm_{0.3}Fe_{10}Si_2$ compound (no detectible impurities). As the v_s increases, the XRD peaks become broader indicating that the 1:12 crystallites become smaller. This apparent refinement is consistent with the accompanying increase in the coercivity H_c, which is shown in Fig. 5. When the v_s is increased to 20 m/s for the $Zr_{8.4}Fe_{76.2}Si_{15.4}$ or to 25 m/s for the $Zr_{5.6}Sm_{2.5}Fe_{76.2}Si_{15.4}$, the 1:12 *superstructure* reflections can no longer be detected in the XRD spectra. Solidification at these high cooling rates suppresses ordering of the Fe(Si) atom pairs producing the $TbCu_7$-type structures instead of the 1:12. The XRD data for the v_s = 25 m/s (Fig. 4) may be interpreted as $TbCu_7$-type structures with a = 0.475 nm, c = 0.418 nm (the Sm-free alloy) and a = 0.478 nm, c = 0.419 nm (Sm-substituted). Because the ordering can be partial or inhomogeneous throughout the sample, the disappearance of the 1:12 structure with v_s should be gradual. It is probably this gradual disappearance of the hard magnetic phase that is responsible for the eventual decline of the coercivity at the higher v_s values. In the as-spun samples, the coercivity associated with the Sm-substituted 1:12 compound is expectably higher than for the Sm-free 1:12, but it remains rather low, never reaching even 1 kOe.

Higher H_c values could be obtained through annealing of the "overquenched" alloys having the $TbCu_7$-type structure as their principal phase (annealing of *amorphous* alloys was not attempted in this work, because it was not expected to produce the 1:12 structure [19]). The XRD data, including those shown in Fig. 4, confirm the re-emergence of the ordered 1:12 structure when these alloys are annealed. The crystallites observed in the middle of cross-sectioned optimally processed alloys can be seen in the micrographs shown in Fig. 6; they are typically 30 to 70 nm in size. The maximum H_c of 0.7 kOe was attained in an annealed $Zr_{8.4}Fe_{76.2}Si_{15.4}$ alloy (Fig. 7a) with a noticeably increased amount of the bcc Fe-Si and $Zr_6Fe_{16}Si_7$ phases (Fig. 4a). Even a larger amount of bcc phase was observed after a longer-than-optimum annealing (XRD data not shown). Thus, it appears that the development of the coercivity in this case is limited by decomposition of the metastable $ZrFe_{10}Si_2$ compound [12]. If the properties of this nanocrystalline rare-earth-free alloy could be preserved/reproduced in a three-dimensional magnet, the latter would exhibit a remanence B_r of 6 kG and a maximum energy product $(BH)_{max}$ of 1.4 MGOe.

For the optimally annealed $Zr_{5.6}Sm_{2.5}Fe_{76.2}Si_{15.4}$, a calculated B_r of 6.3 kG is only marginally higher. However, because of a more than tripled H_c of 2.4 kOe (Fig. 7b), a calculated $(BH)_{max}$ of this alloy reaches 4.6 MGOe. Although the H_c is still rather low, as a fraction of the H_a it is higher than the one reported for the melt-spun $SmFe_{10}Si_2$ [13], 5.9% compared to 3.3%. It may be also noted that the XRD characterization of the annealed $Zr_{5.6}Sm_{2.5}Fe_{76.2}Si_{15.4}$ reveals little, if any, signs that decomposition of the 1:12 structure had already begun, and the coercivity is more likely to be limited by growth of the 1:12 crystallites. Therefore, introduction of grain growth inhibitors, such as fine precipitates of carbides or borides of the refractory elements, may be expected to further improve the H_c and $(BH)_{max}$ of the Sm-substituted nanocrystalline alloy.

4. Conclusion

Moderate Sm substitutions for Zr dramatically increase the magnetocrystalline anisotropy of the $ZrFe_{10}Si_2$ compound. At only 2.3 at.% of the rare earth, an anisotropy of the $Zr_{0.7}Sm_{0.3}Fe_{10}Si_2$ compound is strong enough to enable the development of an efficient permanent magnet. Although the melt-spinning experiments have confirmed the effect of Sm, this method has not yet produced a material superior to the ferrite magnets. A technique yielding crystallographically

anisotropic $Zr_{1-x}Sm_xFe_{10}Si_2$ alloys with a higher H_c/H_a ratio must be discovered to make these very rare-earth-lean materials competitive as permanent magnets.

Acknowledgments

This work was supported by the US Department of Energy (Grant No. DE-FG02-04ER4612) and University of Delaware Energy Institute.

References

[1] K.H.J. Buschow, Permanent magnet materials based on tetragonal rare earth compounds of the type $RFe_{12-x}M_x$, J. Magn. Magn. Mater. 100 (1991) 79–89.

[2] Y.Z. Wang, G.C. Hadjipanayis, Magnetic properties of Sm-Fe-Ti-V alloys, J. Magn. Magn. Mater. 87 (1990) 375–378.

[3] L. Schultz, K. Schnitzke, J. Wecker, High coercivity in mechanically alloyed Sm-Fe-V magnets with a $ThMn_{12}$ crystal structure, Appl. Phys. Lett. 56 (1990) 868–870.

[4] M. Okada, A.Kojima, K. Yamagishi, M. Homma, High coercivity in melt-spun $SmFe_{10}(Ti,M)_2$ ribbons (M = V/Cr/Mn/Mo), IEEE Trans. Magn. 26 (1990) 1376–1378.

[5] L. Schultz, K. Schnitzke, J. Wecker, M. Katter, C. Kuhrt, Permanent magnets by mechanical alloying, J. Appl. Phys. 70 (1991) 6339-6344.

[6] M. Endoh, K. Nakamura and H. Mikami, Nd(Fe,Mo)12Nx compounds and magnets, IEEE Trans. Magn. 28 (1992) 2560-2562.

[7] Y.C. Yang, J. Yang, J.Z. Han, C.S. Wang, S.Q. Liu, H.L. Du, Research and development of interstitial compounds, IEEE Trans. Magn. 51 (2015) 2103806.

[8] N. Drebov, A. Martinez-Limia, L. Kunz, A. Gola, T. Shigematsu, T. Eckl, P. Gumbsch, C. Elsässer, Ab initio screening methodology applied to the search for new permanent magnetic materials, New J. Phys. 15 (2013) 125023 (1–24).

[9] D. Goll, R. Loeffler, R. Stein, U. Pflanz, S. Goeb, R. Karimi, G. Schneider, Temperature dependent magnetic properties and application potential of intermetallic $Fe_{11-x}Co_xTiCe$, Phys. Status Solidi RRL 8 (2014) 862–865.

[10] C. Zhou, K. Sun, F.E. Pinkerton, M.J. Kramer, Magnetic hardening of $Ce_{11+x}Fe_{11-y}Co_yTi$ with $ThMn_{12}$ structure by melt spinning, J. Appl. Phys. 117 (2015) 17A741 (1–4).

[11] A. Tukker, Rare earth elements supply restrictions: market failures, not scarcity, hamper their current use in high-tech applications, Environ. Sci. Technol. 48 (2014) 9973−9974.

[12] A.M. Gabay, G.C. Hadjipanayis, $ThMn_{12}$-type structure and uniaxial magnetic anisotropy in $ZrFe_{10}Si_2$ and $Zr_{1-x}Ce_xFe_{10}Si_2$ alloys, J. Alloys Compd. 657 (2016) 133-137.

[13] M. Solzi, R.H. Xue, L. Pareti, Magnetic anisotropy and first-order magnetization process in $Sm(Fe_{1-x}Co_x)_{10}M_2$ (M = Ti, Si) compounds, J. Magn. Magn. Mater. 88 (1990) 44–50.

[14] W. Kraus, G. Nolze, Powder Cell - a program for the representation and manipulation of crystal structures and calculation of the resulting X-ray powder patterns, J. Appl. Crystallogr. 29 (1996) 301–303.

[15] G. Asti, S. Rinaldi, Nonanaliticity of the magnetization curve: application to the measurement of anisotropy in polycrystalline samples, Phys. Rev. Lett. 28 (1972) 1584-1586.

[16] T.T.M. Palstra, J.A. Mydosh, G.J. Nieuwenhuys, A.M. van der Kraan, K.H.J. Buschow, Study of the critical behavior of the magnetization and electrical resistivity in cubic $La(Fe,Si)_{13}$ compounds, J. Magn. Magn. Mater. 36 (1983) 290-296.

[17] B. Malaman, G. Venturini, A. Blaise, J.P. Sanchez, G. Amoretti, "Magnetic study of $PrFe_2Si_2$ and $PrFe_2Ge_2$ compounds by susceptibility measurements, neutron diffraction, and Mössbauer spectroscopy," Phys. Rev. B 47 (1993) 8681–8690.

[18] R. Skomski, J.M.D. Coey, Magnetic anisotropy — How much is enough for a permanent magnet? Scr. Mater. 112 (2016) 3–8.

[19] J. Ding, M. Rosenberg, Magnetic properties of melt spun and crystallized $SmFe_{10}M_2$, J. Magn. Magn. Mater. 83 (1990) 257–258.

Table I. Crystallographic and magnetic properties of $ThMn_{12}$-type $Zr_{0.7}R_{0.3}Fe_{10}Si_2$ compounds in arc-melted $Zr_{5.6}R_{2.5}Fe_{76.2}Si_{15.4}$ alloys

R	*a* (nm)	*c* (nm)	Purity[2] (vol.%)	$4\pi M_s$ (kG)	T_C (°C)	H_a (kOe)	$(H_a/8\pi M_s)^{1/2}$
Zr	0.8300[1]	0.4721[1]	96.3	11.4	325[1]	18.7	0.91
Y	0.8323	0.4729	96.8	11.7	291	19.7	0.92
Ce	0.8334	0.4731	98.5	11.6	291	21.1	0.95
Pr	0.8335	0.4728	98.2	11.5	297	11.1	0.70
Sm	0.8340	0.4733	96.9	11.8	310	40.7	1.31

[1]from Ref. 12.

[2]fraction of the 1:12 compound derived from the XRD data.

Figure captions

Fig. 1. XRD spectra of arc-melted $Zr_{5.9}R_{2.5}Fe_{76.2}Si_{15.4}$ alloys. The following structure types (phases) were identified: 1 – $ThMn_{12}$ ($Zr_{0.7}R_{0.3}Fe_{10}Si_2$), 2 - $Mg_6Cu_{16}Si_7$ ($Zr_6Fe_{16}Si_7$), 3 –$NaZn_{13}$ ($LaFe_{13-y}Si_y$), 4 – bcc (Fe-Si), 5 – $BaAl_4$ ($PrFe_2Si_2$).

Fig. 2. Characterization of $Zr_{20.7}Fe_{55.2}Si_{24.1}$ ($Zr_6Fe_{16}Si_7$) alloy annealed for 60 h at 1100 °C: (a) XRD spectrum and (b) room-temperature magnetization curve. The ferromagnetic magnetization M_{FM} is too small to be associated with the principal $Zr_6Fe_{16}Si_7$ phase.

Fig. 3. Second derivative of magnetization for arc-melted $Zr_{5.6}R_{2.5}Fe_{76.2}Si_{15.4}$ alloys. The anisotropy fields can be obtained from the peak positions after correction for the self-demagnetization.

Fig. 4. XRD spectra of as-prepared and optimally annealed melt-spun alloys: (a) $Zr_{8.4}Fe_{76.2}Si_{15.4}$, (b) $Zr_{5.6}Sm_{2.5}Fe_{76.2}Si_{15.4}$. The following structure types (phases) were identified: 1 – $ThMn_{12}$ ($Zr_{1-x}Sm_xFe_{10}Si_2$), 2 - $Mg_6Cu_{16}Si_7$ ($Zr_6Fe_{16}Si_7$), 3 – bcc (Fe-Si), 4 – $TbCu_7$.

Fig. 5. Effect of wheel speed on coercivity of as-prepared melt-spun alloys: 1 - $Zr_{8.4}Fe_{76.2}Si_{15.4}$, 2 - $Zr_{5.6}Sm_{2.5}Fe_{76.2}Si_{15.4}$.

Fig. 6. SEM micrographs of fractured surfaces of optimally annealed melt-spun alloys: (a) $Zr_{8.4}Fe_{76.2}Si_{15.4}$ (750 °C, 60 min), (b) $Zr_{5.6}Sm_{2.5}Fe_{76.2}Si_{15.4}$ (850 °C, 20 min).

Fig. 7. Magnetic hysteresis loops of as-prepared and optimally annealed melt-spun alloys: (a) $Zr_{8.4}Fe_{76.2}Si_{15.4}$, (b) $Zr_{5.6}Sm_{2.5}Fe_{76.2}Si_{15.4}$.

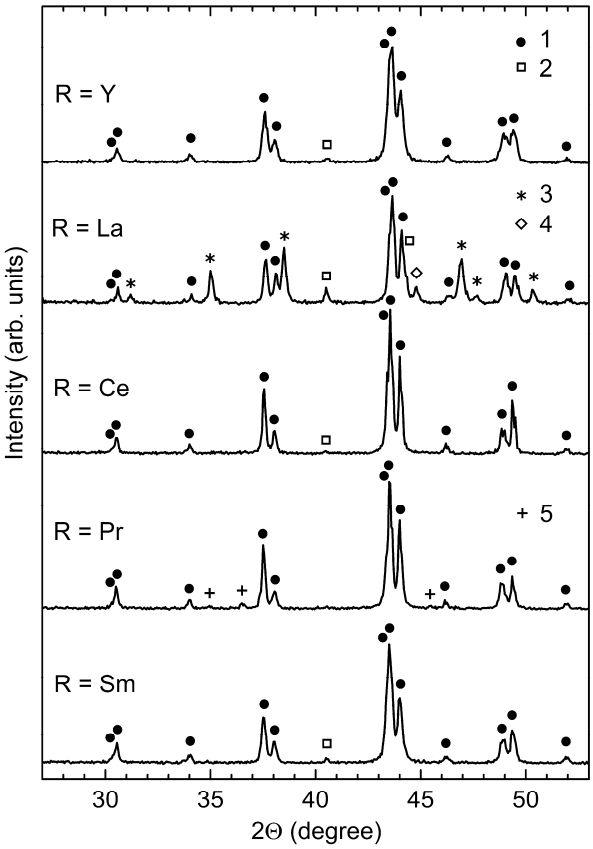

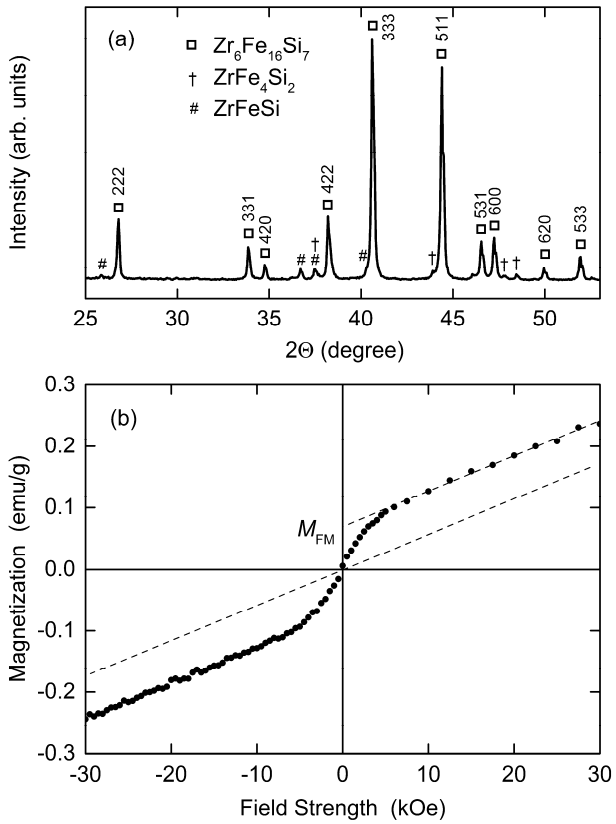

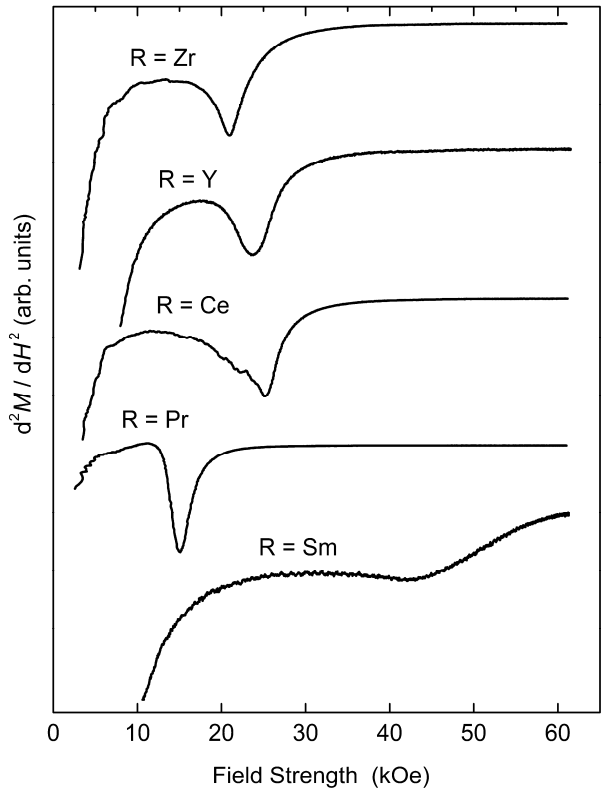

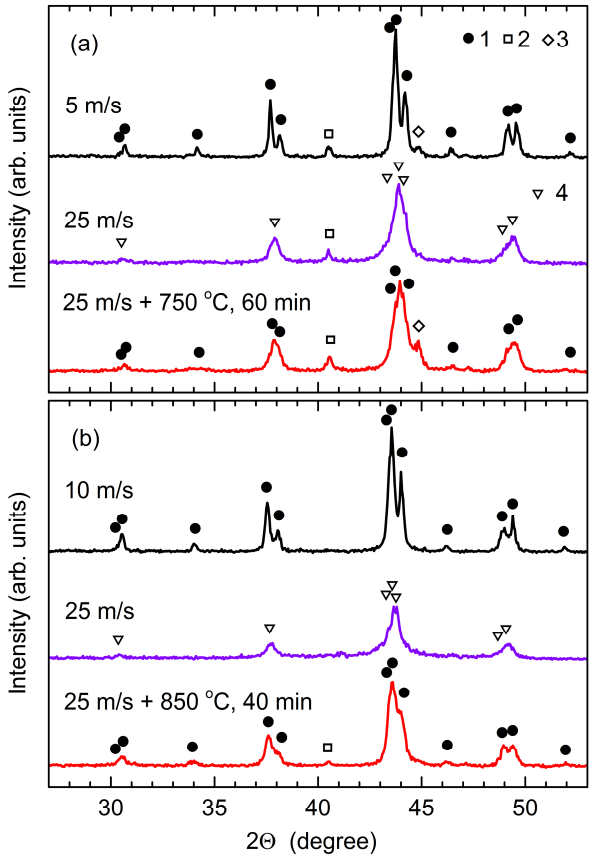

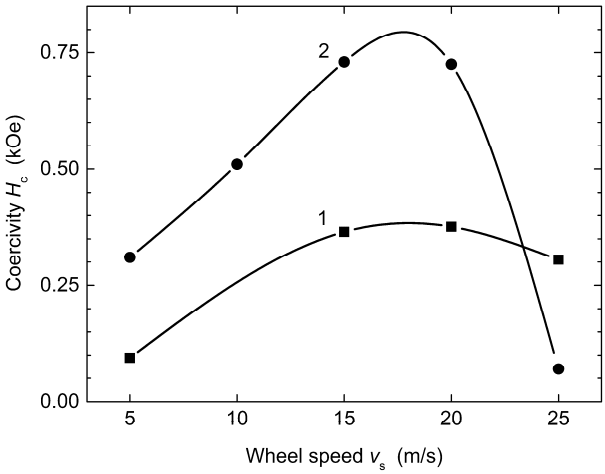

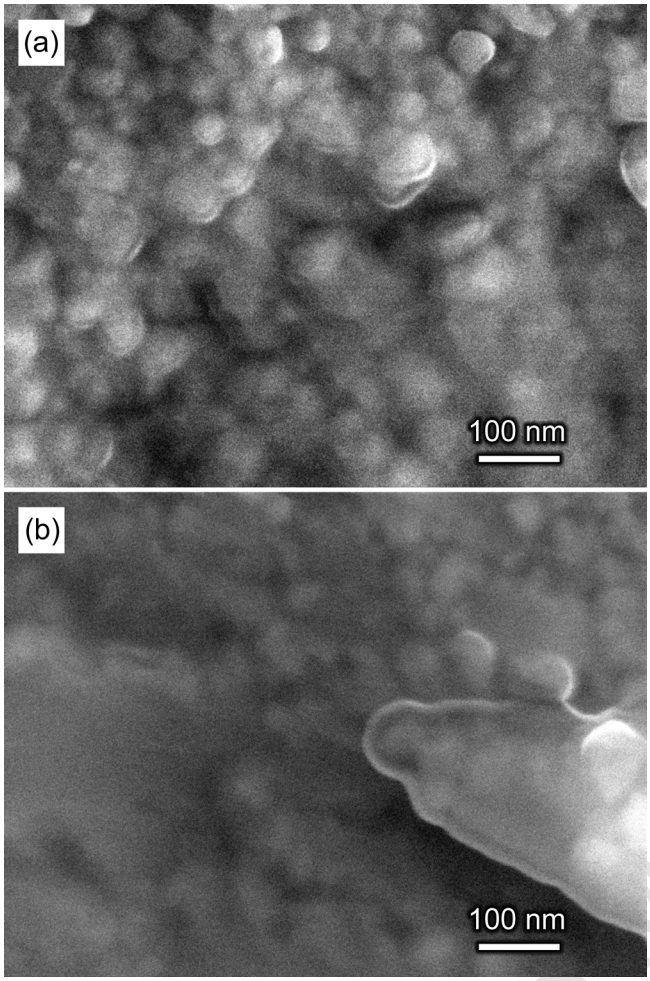

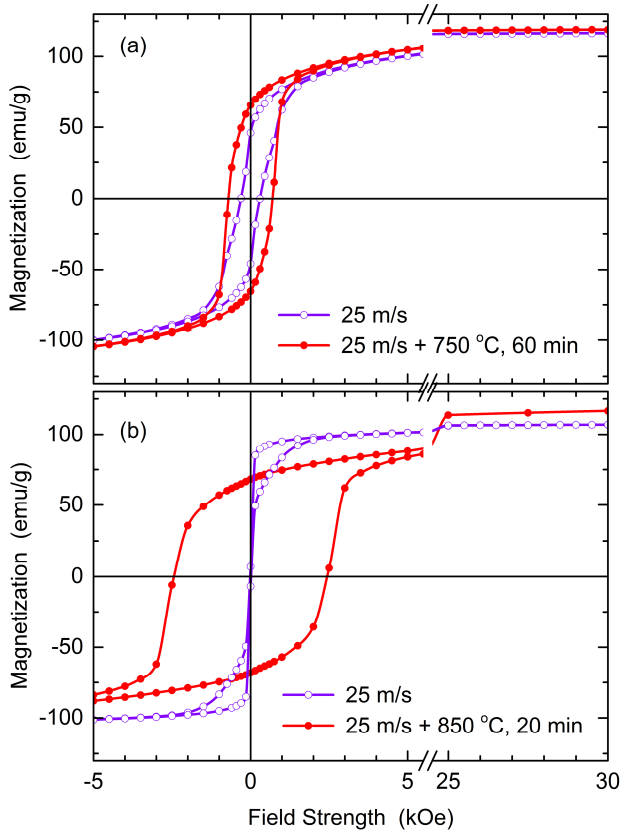

- $ThMn_{12}$-type $Zr_{0.7}R_{0.3}Fe_{10}Si_2$ structure forms with Y, Ce, Pr, Sm, but not with La.
- 30% Sm substitution for Zr increases the anisotropy field by 120%.
- The $Zr_{0.7}Sm_{0.3}Fe_{10}Si_2$ compound has a magnetic hardness parameter of 1.3.
- The effect of Sm is confirmed in melt-spun nanocrystalline alloys.